© 2023. Published by The Company of Biologists Ltd | Journal of Cell Science (2023) 136, jcs260216. doi:10.1242/jcs.260216

RESEARCH ARTICLE

Cardiomyocyte differentiation from human induced pluripotent stem cells is delayed following knockout of Bcl-2

Tim Vervliet[1,*], Robin Duelen[2], Ankit Pradhan[3], Rita La Rovere[1], H. Llewelyn Roderick[3] and Maurilio Sampaolesi[2]

ABSTRACT

Anti-apoptotic B-cell lymphoma 2 (Bcl-2) regulates a wide array of cellular functions involved in cell death, cell survival and autophagy. Less known is its involvement in the differentiation of cardiomyocytes. As a consequence, mechanisms by which Bcl-2 contributes to cardiac differentiation remain to be elucidated. To address this, we used CRISPR/Cas9 to knockout (KO) *BCL2* in human induced pluripotent stem cells (hiPSCs) and investigated the consequence of this KO for differentiation towards cardiomyocytes. Our results indicate that differentiation of hiPSCs to cardiomyocytes was delayed following *BCL2* KO. This was not related to the canonical anti-apoptotic function of Bcl-2. This delay led to reduced expression and activity of the cardiomyocyte Ca^{2+} toolkit. Finally, Bcl-2 KO reduced c-Myc expression and nuclear localization in the early phase of the cardiac differentiation process, which accounts at least in part for the observed delay in the cardiac differentiation. These results suggest that there is a central role for Bcl-2 in cardiomyocyte differentiation and maturation.

KEY WORDS: Bcl-2, Ca^{2+} signaling, Cardiomyocyte differentiation, Human induced pluripotent stem cells

INTRODUCTION

B-cell lymphoma 2 (Bcl-2) is involved in the regulation of cell death and survival decisions at multiple levels. Canonically, the anti-apoptotic Bcl-2 protein binds to pro-apoptotic Bcl-2-family members, such as Bax and Bak (also known as BAX and BAK1), thereby inhibiting their pro-apoptotic functions as inducers of mitochondrial outer membrane permeabilization (MOMP) and leading to cytochrome *c* release (Brunelle and Letai, 2009). In addition, Bcl-2 modulates inositol-1,4,5-trisphosphate receptors (IP_3Rs) thus, inhibiting pro-apoptotic Ca^{2+} signalling towards the mitochondria (Rong et al., 2008). Other Ca^{2+}-handling proteins targeted by Bcl-2 include ryanodine receptors (RyRs), sarco/endoplasmic reticulum ATPases and voltage-dependent anion channels (Vervliet et al., 2016). Besides regulating the apoptotic outcome, Bcl-2 is involved in modulating autophagic flux. For instance, Bcl-2 associates with Beclin 1, thereby limiting the initiation of autophagosome formation and thus autophagic flux (Pattingre et al., 2005).

Regulation of cell death and survival is also key during differentiation. Consistent with this, Bcl-2 is involved in the differentiation of certain cells and tissues. For instance, neuronal differentiation has been shown to be regulated by Bcl-2. Transplanting embryonic stem cells overexpressing Bcl-2 in rat cortex enhanced recovery and neuronal differentiation after ischaemic insult (Wei et al., 2005). In addition, overexpression of Bcl-2 in the PC12 neural crest tumour cell line, led to increased expression of genes associated with neural differentiation, whereas it decreased expression of proliferation-related genes (Liang et al., 2003). In the heart, Bcl-2 has been shown to be upregulated in a GATA4-dependent manner (Kobayashi et al., 2006), suggesting a role in cardiac development. The latter is further supported by the increased cardiomyocyte proliferation seen in mice overexpressing Bcl-2 in the heart (Limana et al., 2002). However, the molecular pathways underlying Bcl-2 regulation of cardiomyocyte differentiation have not been investigated.

Bcl-2 is phosphorylated at a number of sites resulting in modulation of its function. For example, Thr56, Ser70 and Ser87 located in the Bcl-2 unstructured loop are targets of multiple kinases, including members of the mitogen-activated protein kinases (MAPK) family of kinases (Maundrell et al., 1997; Blagosklonny, 2001; De Chiara et al., 2006). For example, phosphorylation of Bcl-2 by p38MAPK (herein referring to the p38MAPK family) was demonstrated to induce apoptosis by inhibiting the anti-apoptotic function of Bcl-2 and inducing it to trigger the release of cytochrome *c* following MOMP induction in response to acute stressors (De Chiara et al., 2006). Phosphorylation of Bcl-2 has also been shown to result in its translocation to the nucleus (Zhou et al., 2017). In the nucleus, Bcl-2 interacts with c-Myc, increasing the stability and transcriptional activity of the latter (Jin et al., 2006). These functional interactions between Bcl-2, p38MAPK and c-Myc could also play a key role in the heart. Indeed, p38MAPK is involved in the commitment of mouse embryonic stem cells to differentiate into cardiomyocytes (Aouadi et al., 2006) and regulates cardiomyocyte proliferation (Engel et al., 2005). Moreover, cardiac c-Myc overexpression in mice increases cardiac mass and hyperplasia without detrimental effects on cardiomyocyte maturation (Jackson et al., 1990).

In this study, we aim to further unravel the function of Bcl-2 in cardiomyocyte differentiation. To this end, we analysed the effect of CRISPR/Cas9-mediated *BCL2* knockout (KO) on the derivation of cardiomyocytes through differentiation from human induced pluripotent stem cells (hiPSCs). We show that the temporal trajectory of hiPSC differentiation towards cardiomyocytes is delayed by *BCL2* KO, which resulted in functional changes. Furthermore, we showed that Bcl-2 KO cells have reduced c-Myc expression and nuclear localization during early cardiomyocyte differentiation compared to that in control cells. Moreover, in

[1]Laboratory of Molecular and Cellular Signaling, Department of Cellular and Molecular Medicine, KU Leuven, 3000 Leuven, Belgium. [2]Translational Cardiomyology Laboratory, Department of Development and Regeneration, KU Leuven, 3000 Leuven, Belgium. [3]Laboratory of Experimental Cardiology, Department of Cardiovascular Sciences, KU Leuven, 3000 Leuven, Belgium.

*Author for correspondence (tim.vervliet@kuleuven.be)

T.V., 0000-0002-4030-5875; R.D., 0000-0003-0904-1215; A.P., 0000-0003-3090-9066; H.L.R., 0000-0001-7065-3523

Handling Editor: John Heath
Received 6 May 2022; Accepted 15 December 2022

Journal of Cell Science (2023) 136, jcs260216. doi:10.1242/jcs.260216

control cells, upregulation of c-Myc expression coincided with increased Bcl-2 levels. Together, these results support a critical role for Bcl-2 in the generation of cardiomyocyte differentiation from hiPSCs and suggest a role for it in the development of cardiomyocytes.

RESULTS

Creation and validation of Bcl-2 KO hiPSCs

BCL2 KO was performed in the commercially available Gibco™ Episomal hiPSC Line (A18945) using a CRISPR/Cas9-based approach. Single-guide RNAs (sgRNAs) were designed to induce Cas9-mediated double-stranded breaks (DSBs) in the genomic DNA of hiPSCs. sgRNA specificity and CRISPR/Cas9 DSB cutting were evaluated in HEK293T cells. The most promising *BCL2*-targeting sgRNA, designed to target an early sequence in the *BCL2* gene, was selected. Cas9-mediated gene editing was performed via homology-directed repair, using a plasmid-based donor template with homology arms for the *BCL2* gene region of interest, flanking a GFP-Hygromycin-TK expressing cassette for selection. Stop codon-introducing point mutations, inserting a premature stop codon in the *BCL2* gene, were introduced in one of the homology arm regions, in order to introduce mutations in the *BCL2* gene. After antibiotic selection and single-cell colony isolation, the presence of the hygromycin cassette at the correct genomic locus was validated. Next, the hygromycin cassette was removed following PiggyBac excision and fialuridine (FIAU) selection, resulting in completely gene-editing-free Bcl-2 KO hiPSC lines. Sequencing analysis of the *BCL2* gene confirmed CRISPR/Cas9-mediated alterations in the *BCL2* gene. In Fig. 1, we restricted the validation to two clones, Bcl-2 KO1 and Bcl-2 KO2, which were used in this study. At the genomic level, all tested clones were characterized by a base pair deletion or frame shift mutation in the *BCL2* gene. The majority of the tested clones exhibited a deletion of 4 base pairs (Fig. 1A), resulting in the introduction of three premature stop codons at the protein level (Fig. 1B). Verification at the protein level via immunoblotting showed the absence of endogenous Bcl-2 in both clones (Fig. 1C), suggesting a complete KO of the *BCL2* gene. Finally, we screened for potential CRISPR/Cas9 off-target effects based on the sequence homology of the used sgRNAs (Fig. 1D). In both clones, no alterations near the potential off-target sites were detected, showing no unwanted Cas9-mediated DSB cuts.

Bcl-2 KO does not inhibit but delays the induction of cardiac differentiation

After validation and selection of two Bcl-2 KO clones, we determined the effects of Bcl-2 KO on cardiomyocyte differentiation. The differentiation scheme utilized in this study is depicted in Fig. 2A. A commercial cardiomyocyte differentiation kit was utilized and resulted in the robust generation of cardiomyocyte cultures.

Consistent with the manufacturer's instructions using this protocol, large areas of spontaneously beating cardiomyocytes were observed as early as day 7 in the control differentiation. In the Bcl-2 KO clones, spontaneous beating was not seen until at least 9 days after the induction of differentiation. Moreover, the regions of spontaneously active cardiomyocytes were scarcer and smaller (see also Fig. 4A,B). This would suggest that Bcl-2 KO impacts cardiac differentiation. To investigate this further, we first assessed whether Bcl-2 KO resulted in impaired induction of expression of early and late cardiomyocyte differentiation markers (Fig. 2B). In control and Bcl-2 KO conditions, real-time quantitative PCR (RT-qPCR) analysis revealed a decrease in expression of pluripotency markers upon differentiation as expected. mRNA expression of the mesodermal marker *BRACH* (also known as *TBXT*), indicative of mesoderm induction, occurred as anticipated on day 2 of differentiation for both control and KO conditions. Consistent with their expected upregulation during early cardiac differentiation, *NKX2.5* (also known as *NKX2-5*) and *GATA4* were increased in expression at day 7 and remained elevated for the remainder of the control differentiation. However, in both Bcl-2 KO lines, *NKX2.5* and *GATA4* showed significantly lower expression levels at day 7, which for *NKX2.5*, but not for *GATA4*, recovered at 14 days of differentiation. A similar trend was observed in two (*MYH6* and *TNNI3*) out of three (*TNNT2*) tested late-stage cardiomyocyte differentiation markers. This delaying of cardiomyocyte differentiation upon Bcl-2 KO either suggests that Bcl-2 is required for the efficient upregulation of cardiac differentiation markers or that Bcl-2 contributes to increasing and/or maintaining the number of differentiated cardiomyocytes, which in turn mediates the increased expression of these cardiac differentiation markers.

To further support these observations and show that KO of Bcl-2 does not impair cardiomyocyte differentiation from hiPSC cultures, cardiomyocytes were immunostained for cardiac troponin T (cTnT, encoded by *TNNT2*) after 14 days of differentiation. In both control and KO conditions, we were able to detect areas of cTnT staining (Fig. 2C,D), supporting the observation that KO of Bcl-2 does not completely prevent the differentiation of cardiomyocytes from hiPSCs.

Bcl-2 KO does not trigger cell death induction or changes in the induction of autophagy in hiPSC-derived cardiomyocytes

One explanation for the lower expression of cardiac progenitor and cardiomyocyte markers in the Bcl-2 KO conditions is that loss of Bcl-2 results in increased cell death, leading to a lower number of differentiated cells and an impact on population measures of differentiation. This is plausible as Bcl-2 is known to play important functions in apoptosis and autophagy, two pathways that can control cell numbers (Brunelle and Letai, 2009; Pattingre et al., 2005).

Bcl-2 is a key anti-apoptotic protein, known to bind to and inhibit pro-apoptotic Bax and Bak, crucial for the execution of apoptosis (Brunelle and Letai, 2009). Therefore, KO of Bcl-2 might lead to increased apoptotic cell death. In order to address this, we performed immunoblot analysis in which we probed for poly ADP-ribose polymerase (PARP; also known as PARP1), which is cleaved by active caspase 3, an effector of apoptosis downstream of Bax and Bak activation. No difference in the ratio of the cleaved to total PARP was observed between control and Bcl-2 KO lines, indicating no increase in caspase 3 activity (Fig. 3A). To further support this, a more quantitative method for determining the levels of cell death was performed. Bcl-2 KO and control cells were differentiated for 0, 7, 14 and 21 days and were co-stained with NucView®488, propidium iodide and a cell-permeable Hoechst 33342 dye to monitor caspase 3 activation, cell integrity and total nucleus count, respectively. All these dyes when active or present in the cell bind to nuclear DNA, allowing their quantification relative to the total nuclear fluorescence of the Hoechst 33342 stain. Cells that were positive for either NucView®488 or NucView®488 together with propidium iodide were classified as apoptotic, whereas cells positive for propidium iodide only, were classified as necrotic. For each day of experiments, a staurosporine-treated control condition was used to set the threshold for cells being positive for NucView®488 and propidium iodide staining. Representative images for each differentiation day and the tested conditions can be found as Figs S1–S4. Quantifying these experiments showed no significant differences in basal levels of

Journal of Cell Science (2023) 136, jcs260216. doi:10.1242/jcs.260216

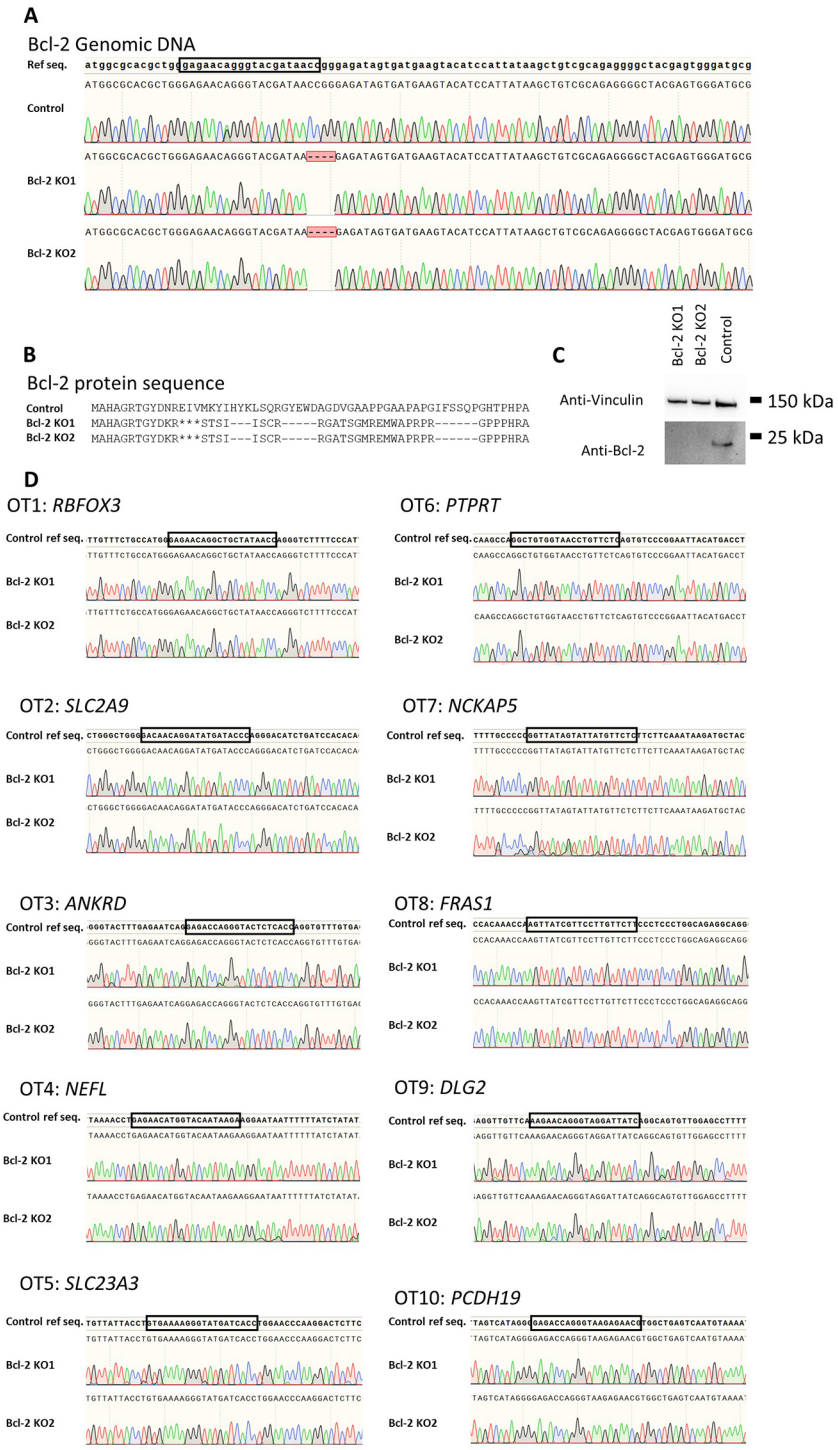

Fig. 1. CRISPR/Cas9-mediated KO of Bcl-2 in hiPSCs. (A) Sanger sequencing of the first 100 base pairs of the genomic *BCL2* open reading frame comparing the sequence of the control condition to the two Bcl-2 KO hiPSC clones utilized in this study. The utilized sgRNA is indicated by the black box in the *BCL2* reference sequence (ref seq.) with accession number NM_000633.3. (B) Predicted protein sequence based on the sequencing result obtained in A for the control and Bcl-2 KO hiPSCs. * indicates the presence of a premature stop codons. (C) Immunoblot validating the absence of Bcl-2 in the Bcl-2 KO clones compared to the control. Image representative of at least three repeats. (D) Sequencing results surrounding the 10 most likely off-target (OT) genes associated with the utilized sgRNA. The potential off-target is indicated by the black box in the ref seq. All DNA sequences and profiles were visualized using SnapGene® software.

either apoptosis or necrosis between control and Bcl-2 KO conditions (Fig. 3B), confirming the PARP findings in Fig. 3A. Of note, early in the differentiation (day 7) there appeared to be more necrosis in all conditions compared to what was seen at later stages of differentiation (day 14 and 21) where apoptosis induction was more pronounced.

Bcl-2 also plays important roles in the regulation of autophagy. By binding to Beclin 1 for instance, Bcl-2 impairs the induction of autophagosome formation thus potentially inhibiting autophagy induction (Pattingre et al., 2005). In order to measure autophagy induction, we monitored the levels of lipidated microtubule-associated protein light chain 3 family proteins (LC3-II; the lipidated form of MAP1LC3B). No difference in LC3-II levels could be detected between control and Bcl-2 KO clones (Fig. 3C). In addition, we also monitored mammalian target of rapamycin (mTOR) activity by determining the phosphorylation state/activity of p70 S6 kinase (encoded by *RPS6KB1*) (Fig. 3C), a downstream target of mTOR. Similar to the LC3-II results, the phosphorylation state of p70 S6 kinase was unaltered, confirming that Bcl-2 KO did not alter basal autophagic induction.

Finally, we validated whether the Bcl-2 KO clones could upregulate the closely related anti-apoptotic Bcl-X_L (encoded by

Journal of Cell Science (2023) 136, jcs260216. doi:10.1242/jcs.260216

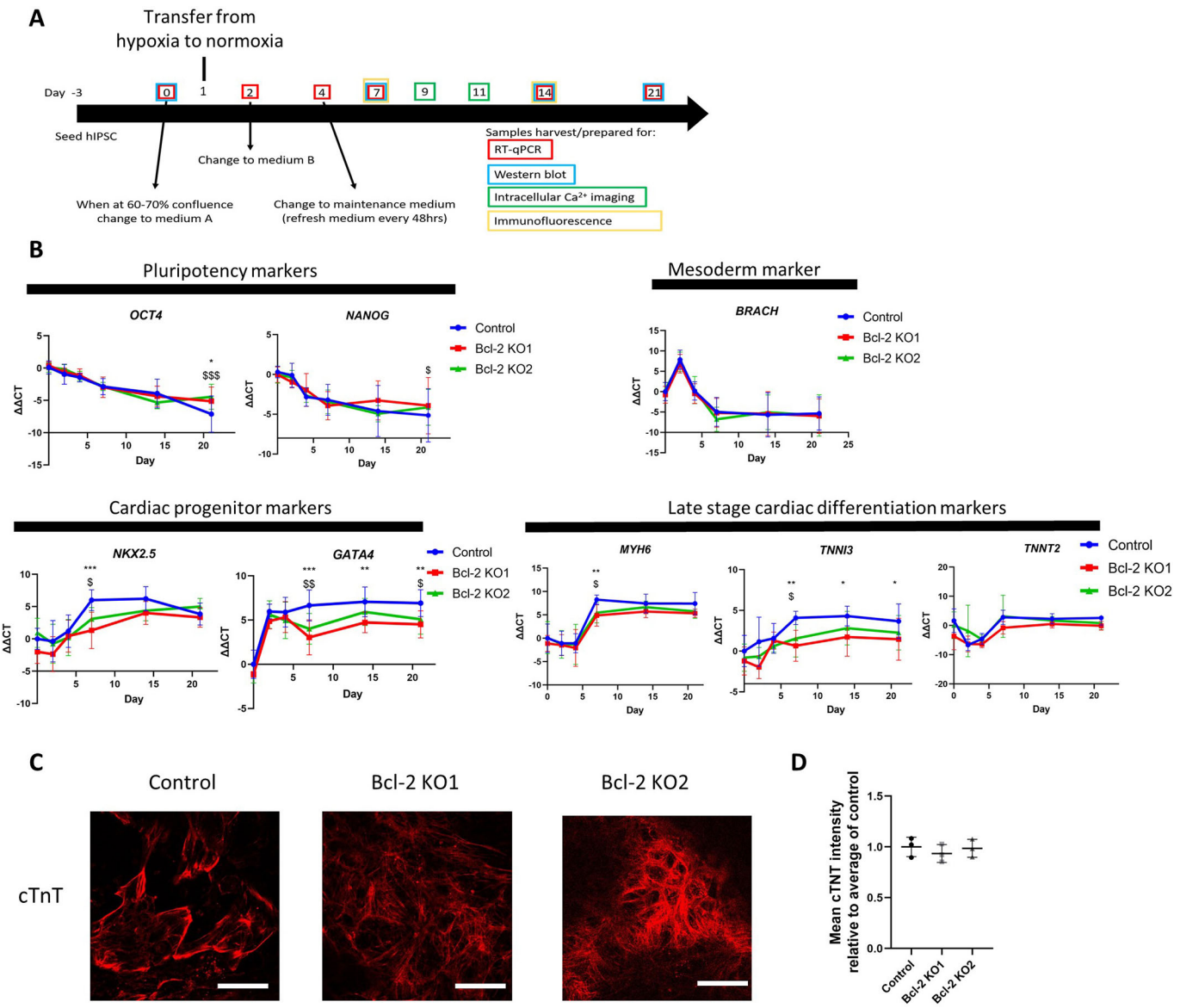

Fig. 2. Bcl-2 KO delays the expression of certain cardiac differentiation markers. (A) Scheme of the cardiac differentiation protocol, and time points where samples were harvested for RT-qPCR, immunoblotting, immunofluorescence staining or utilized for intracellular Ca^{2+} imaging. (B) RT-qPCR analysis of gene expression profile associated with cardiomyocyte differentiation in control and the two Bcl-2 KO clones at time points shown (0, 2, 4, 7 14 and 21 days of differentiation). The data points represent ΔΔCT mean±s.d. values of at least four independent differentiations ($n \geq 4$) of the indicated genes at the indicated time points. * and $ indicate significant difference between control and Bcl-2 KO1 or Bcl-2 KO2, respectively. * or $ indicates $P<0.05$; ** or $$ indicates $P<0.01$, *** or $$$ indicates $P<0.001$ (two-way ANOVA tests with Dunnett post test for multiple comparison). (C) Confocal images of control and Bcl-2 KO cardiomyocytes differentiated for 14 days immunofluorescently stained for cTnT. Experiments were performed three times independently ($n=3$). Scale bars: 50 µm. (D) Quantification of the cTnT signal of the immunofluorescence experiments, comparing control to the Bcl-2 KO lines. Data points depict the mean±s.d. cTnT intensity from all pictures acquired from one independent experiment, relative to the average of the control conditions across all experiments. In total three independent experiments were performed ($n=3$). No significant differences were detected between the conditions after one-way ANOVA testing with Tukey post test.

BCL2L1) protein to compensate for the loss of Bcl-2. However, Bcl-X_L levels were not significantly altered in the Bcl-2 KO clones compared to the control and even seemed to decrease in all conditions rather than increase during differentiation (Fig. 3C).

Bcl-2 KO reduces the area of beating cells and inhibits the amplitude of spontaneous Ca^{2+} transients in hiPSC-derived cardiomyocytes

As the induction of cardiomyocyte differentiation was delayed upon KO of Bcl-2, and no differences were observed in apoptosis and autophagy induction, we next examined whether functional measures of cell physiology were similarly affected in Bcl-2 KO hiPSC-derived cardiomyocytes. To these ends, we investigated spontaneous Ca^{2+} transients, which are responsible for the spontaneous contractions in control and Bcl-2 KO cardiomyocytes, using live-cell Ca^{2+} imaging. Ca^{2+} imaging experiments were performed in cardiomyocytes differentiated for 9 or 11 days. At these time points, it was feasible to detect spontaneously contracting areas in both control and Bcl-2 KO cardiomyocytes. Fluo-4 loading allowed the measuring of the

Journal of Cell Science (2023) 136, jcs260216. doi:10.1242/jcs.260216

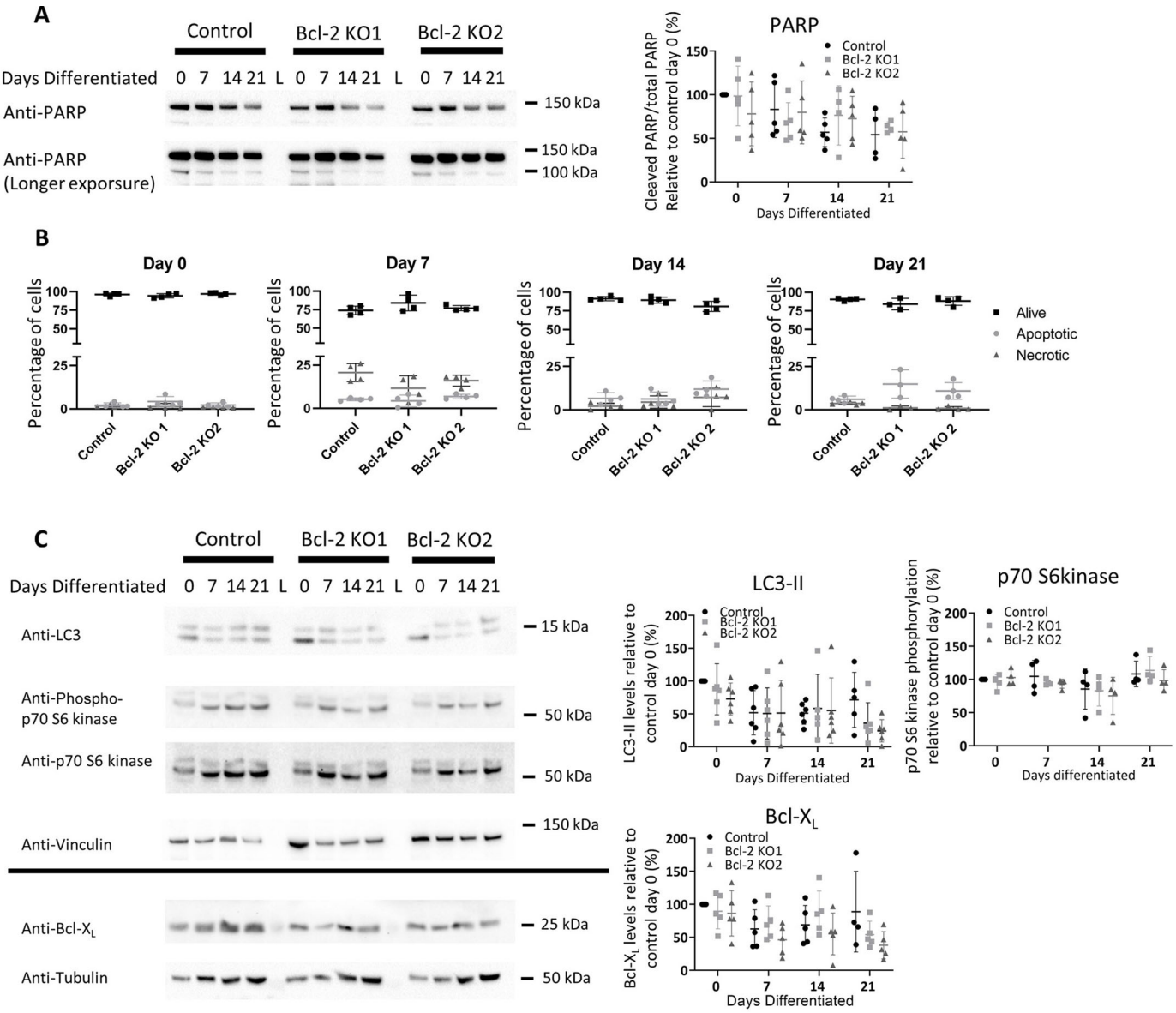

Fig. 3. Basal levels of apoptosis, necrosis and autophagy induction are unaltered upon KO of Bcl-2. (A) immunoblot analysis for the indicated proteins in lysates prepared from cardiomyocytes derived from control or Bcl-2 KO clones differentiated for 0, 7, 14 or 21 days (left panel). L depicts the lane in which molecular mass markers were loaded. Quantification of the performed immunoblot experiments (right panel). The expression levels of cleaved PARP were normalized to the total PARP levels. All protein levels are shown relative to the levels for control day 0. All differentiations were performed at least 4 times ($n \geq 4$) the mean±s.d. is indicated in the figures. For comparing day 0 values, a non-parametric Kruskall–Wallis tests with Dunn's multiple comparison was performed to compare to the normalized control value of control day 0. For all other days, one-way ANOVA tests with Tukey post test for multiple comparison were performed as the assumptions of normality were met in these conditions. (B) Quantification of the performed cell death experiments after 0, 7, 14 and 21 days of differentiation of control and Bcl-2 KO clones. 15 min before image acquisition the cells were co-treated with a cell permeable Hoechst 33342 stain, NucVIEW®488 and propidium iodide. Cells positive for either NucView®488 or both NucView®488 and propidium iodide were identified as apoptotic. Cells only positive for propidium iodide were classified as necrotic. All values were normalized to the total cell count obtained by the cell permeable Hoechst 33342 stain. The experiment was performed at least three times independently and mean±s.d. is shown ($n \geq 3$). One-way ANOVA tests with Tukey post test for multiple comparison were performed as the assumptions of normality were met in all conditions. No significant differences were detected. (C) Immunoblot analysis for the indicated proteins in lysates prepared from cardiomyocytes derived from control or Bcl-2 KO clones differentiated for 0, 7, 14 or 21 days (left panels). The black horizontal line depicts which immunostainings were performed on the same immunoblot. L depicts the lane in which molecular mass markers were loaded. For p70 S6 kinase activity, the phosphorylated p70 S6 kinase levels were divided by the total p70 S6 kinase levels. All other protein expression levels are plotted normalized to their corresponding loading control run on the same immunoblot (vinculin or tubulin). All protein levels are shown relative to the levels for control day 0 (right panels). All differentiations were performed at least four times ($n \geq 4$) the mean±s.d. is indicated in the figures. For comparing day 0 values, a non-parametric Kruskall–Wallis tests with Dunn's multiple comparison was performed to compare to the normalized control value of control day 0. For all other days, one-way ANOVA tests with Tukey-post test for multiple comparison were performed as the assumptions of normality were met in these conditions.

surface area of beating cells by monitoring spontaneous changes in cytosolic [Ca^{2+}]. This analysis was visualized in Fig. 4A as maximum intensity *Z*-projections of the first 30 s (300 images) of example control and Bcl-2 KO conditions. Compared to that observed in controls, the area of spontaneously active cardiomyocytes was severely decreased in Bcl-2 KO cells

Journal of Cell Science (2023) 136, jcs260216. doi:10.1242/jcs.260216

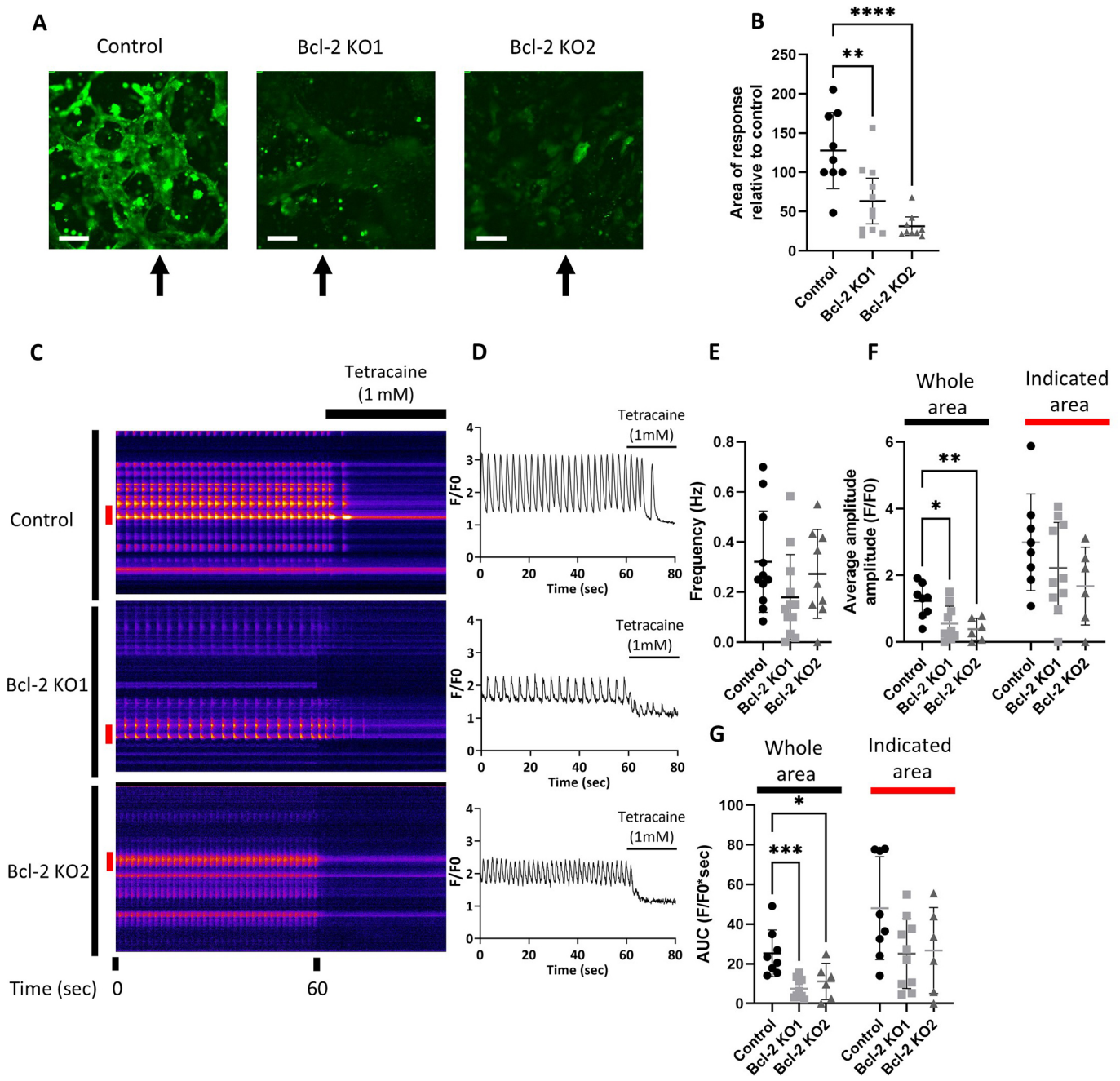

Fig. 4. KO of Bcl-2 reduces the area of spontaneous activity as well as the spontaneous Ca^{2+} release. Spontaneous intracellular Ca^{2+} measurements in cardiomyocytes differentiated for 9 or 11 days using Fluo-4. (A) Maximum intensity projections of the first 30 s (300 images) of a representative Ca^{2+} measurement for control and Bcl-2 KO conditions. Scale bars: 100 µm. The arrows indicate where the line was drawn for 're-slicing' the stack in C. (B) Quantification of the area of spontaneous activity derived from the maximum intensity plots relative to the total area covered by cells (%). Each data point represents the size of the area of spontaneous activity of a single Ca^{2+} imaging experiment. The mean±s.d. are indicated on the graphs. The experiment was performed at least nine times independently for each condition ($n \geq 9$). (C) Visual representation of the experiment showing a time lapse of the pseudo-line scans obtained after re-slicing the image stack for control and Bcl-2 KO conditions. After 60 s, tetracaine (1 mM) was added to block RyR activity and determine the baseline. (D) Intensity profiles obtained by quantifying the entire area (indicated by the black bar left of the pseudo-line scans in C), plotted as F/F_0. F_0 was determined after tetracaine addition. (E–G) Quantification of the spontaneous activity was obtained by determining the frequency (E), amplitude (F) and area under the curve (G). For amplitude and frequency, an additional quantification was performed focussing only on the areas of most intense responses (indicated by the red bar left of the line scans in C). All experiments were performed at least six times ($n \geq 6$). The mean±s.d. are represented on the graphs. For statistical analysis, one-way ANOVA tests with Tukey post test for multiple comparison were performed. *P<0.05, **P<0.01, ***P<0.001, ****P<0.0001.

(Fig. 4B). Next, we focused on the properties of the Ca^{2+} changes. To assess the dynamics of Ca^{2+} transients in these measurements, pseudo-line scans of the largest area of spontaneously active cells were performed spanning the duration of the experiment (Fig. 4C). These analyses were performed by 're-slicing' the entire image stack time series over a vertical line in the image (the arrows in Fig. 4A indicate where these lines were drawn) to generate an xt image. From this line stack, fluorescence intensity measurements

Journal of Cell Science (2023) 136, jcs260216. doi:10.1242/jcs.260216

were made and plotted as normalized fluorescence (F/F_0). This was performed either for the entire slice area (black vertical bar Fig. 4C) or was focussed on the area with the largest response (red bar, Fig. 4C). A representative image of such a line stack for control and Bcl-2 KO clones can be seen in Fig. 4C. The intensity plot of the corresponding line stacks is shown in Fig. 4D. These analyses showed that Bcl-2 KO did not alter the frequency of the spontaneous Ca^{2+} release events compared to the control (Fig. 4E). However, the amplitude (Fig. 4F) and area under the curve (AUC; Fig. 4G) were significantly lower in Bcl-2 KO cardiomyocytes, when quantifying the entire line stack. The data in Fig. 4A,B and the line stack analysis suggest that a larger area of control cardiomyocytes exhibit spontaneous activity compared to in the Bcl-2 KO clones, thus explaining the observed difference. Therefore, we also performed the same quantification but restricted the analysis to the major sites of cell activity (red line in Fig. 4C) and saw that both amplitude and AUC were no longer significantly different between control and Bcl-2 KO. These results confirmed that KO of Bcl-2 did not impair but rather delayed cardiomyocyte differentiation from hiPSCs. These data highlight the advantage of performing imaging experiments in which cell populations of differing maturation can be discretely analysed.

Bcl-2 KO impairs the expression of the cardiac Ca^{2+} toolkit

Our findings suggest that, in the majority of hiPSCs, Bcl-2 KO delayed differentiation into cardiomyocytes and, as a consequence, they did not exhibit spontaneous Ca^{2+} transients and contractions. However, where Bcl-2 KO cells did differentiate, they showed similar functional activity to controls. This suggests that Bcl-2 did not block cardiomyocyte differentiation per se but rather intervened in the decision as to whether hiPSCs differentiate into cardiomyocytes or not. Given the association between the expression of specific Ca^{2+}-handling machinery proteins involved in excitation contraction coupling with cardiomyocyte maturation, we next investigated the underlying mechanisms for this reduced Ca^{2+} signalling capacity. To this end, immunoblot assays were performed to evaluate the expression levels of a number of proteins involved in cardiac function and Ca^{2+} handling (Fig. 5). From these immunoblots, it is clear that the expression levels of RyR2, the sodium Ca^{2+} exchanger (NCX; also known as SLC8A1), the cardiac specific sarco/endoplasmic reticulum ATPase 2A (SERCA2a; also known as ATP2A2) isoform and cTnT were dramatically lower in Bcl-2 KO cardiomyocytes compared to control cardiomyocytes. Inositol 1,4,5-trisphosphate receptor type 2 (IP_3R2) levels showed a similar decline in control and Bcl-2 KO conditions, indicating that the decrease is specific for cardiac-specific markers. These results suggest that when examining the entire cell population in the Bcl-2 KO cultures, only a minority of cells had fully differentiated into cardiomyocytes.

Bcl-2 KO impairs early c-Myc upregulation thereby resulting in reduced functional cardiomyocyte growth

KO of Bcl-2 did not alter the levels of apoptosis or basal autophagy induction. Besides participating in pathways involved in cell removal, Bcl-2 is also involved in the regulation of cellular proliferation differentiation and growth (Liang et al., 2003; Limana et al., 2002; Kobayashi et al., 2006; Wei et al., 2005). An interesting link between Bcl-2 and c-Myc has been described whereby Bcl-2 would stabilize c-Myc thus increasing its expression and activity (Jin et al., 2006). To explore this possibility in hiPSC-derived cardiomyocytes, we determined c-Myc levels in control and Bcl-2 KO lines (Fig. 6A). Interestingly, on differentiation day 7, c-Myc was upregulated in control cells, which was not the case in both Bcl-2 KO conditions. A similar non-significant trend was observed at day 14, whereas at day 21 c-Myc expression in Bcl-2 KO cells recovered to control levels. This observation suggests that loss of Bcl-2 resulted in decreased c-Myc expression during early cardiomyocyte differentiation from hiPSCs.

It has been shown that phosphorylation of Bcl-2 by p38MAPK, a kinase family heavily involved in regulating cell proliferation, leads to the nuclear translocation of Bcl-2, where it provides pro-survival signalling and resistance to chemotherapy (Zhou et al., 2017). This effect of Bcl-2 could at least be in part due to its stabilizing effects on c-Myc in the nucleus, thus promoting c-Myc activity (Jin et al., 2006). To validate the involvement of this pathway on the action of Bcl-2, we determined levels of the active phosphorylated form of p38MAPK and of phosphorylated Bcl-2 by immunoblot analysis (Fig. 6B). Levels of phosphorylated active p38MAPK relative to total p38MAPK levels were not altered between non-differentiated control and Bcl-2 KO cells. However, during differentiation, p38MAPK expression levels significantly increased in control cardiomyocytes, signifying an increase in absolute levels of phosphorylated p38MAPK. No such increase was detected during the differentiation of the Bcl-2 KO cells. Similarly, Bcl-2 phosphorylated at serine 70, a known target of MAPK pathways which facilitates its nuclear translocation (Zhou et al., 2017), was upregulated together with total Bcl-2 throughout the differentiation of control hiPSCs (Fig. 6B). The quantification showed that relative to total Bcl-2 levels, no increase could be observed in Bcl-2 phosphorylation status. However, since both phosphorylated and total Bcl-2 levels clearly increased over time, it can be concluded that the absolute levels of phosphorylated Bcl-2 do increase. Interestingly, in the cardiomyocytes derived from control hiPSCs, Bcl-2 levels were upregulated from day 7 onward, coinciding with the period that has increased levels and/or activity of p38MAPK and c-Myc, highlighting the importance of Bcl-2 for cardiac differentiation.

The above results are in accordance with literature describing a stabilizing effect of Bcl-2 on c-Myc expression in the nucleus, which in turn allows efficient regulation of c-Myc-dependent genes (Jin et al., 2006). In order to further validate whether this is also the case in our cardiomyocyte differentiations, immunofluorescence experiments were setup to determine whether the nuclear c-Myc levels were diminished following Bcl-2 KO (Fig. 7). Given that the largest differences in c-Myc expression were observed at day 7, we focused these experiments on this day. Control and Bcl-2 KO cardiomyocytes differentiated for 7 days were fixed and stained for c-Myc, cTnT and DAPI (Fig. 7, left). Combining the DAPI and c-Myc staining, the intensity and area occupied by c-Myc in the nucleus was quantified (Fig. 7, right). From this analysis, it was clear that both the intensity and area occupied by c-Myc in the nucleus were significantly decreased in Bcl-2 KO condition compared to control. cTnT stain was also imaged to illustrate that cardiac differentiation had started as expected at day 7.

Overall, these results suggest that Bcl-2 KO reduced expression of c-Myc in the early phase of cardiomyocyte differentiation and more specifically lowers the abundance of nuclear c-Myc. As c-Myc is an important regulator of the expression of genes involved in cardiomyocyte differentiation, this could contribute to the delays in the differentiation observed in the Bcl-2 KO hiPSC-derived cardiomyocytes.

DISCUSSION

In this study, we showed that Bcl-2 plays an important role in the early phase of cardiomyocyte differentiation from hiPSCs. KO of

Journal of Cell Science (2023) 136, jcs260216. doi:10.1242/jcs.260216

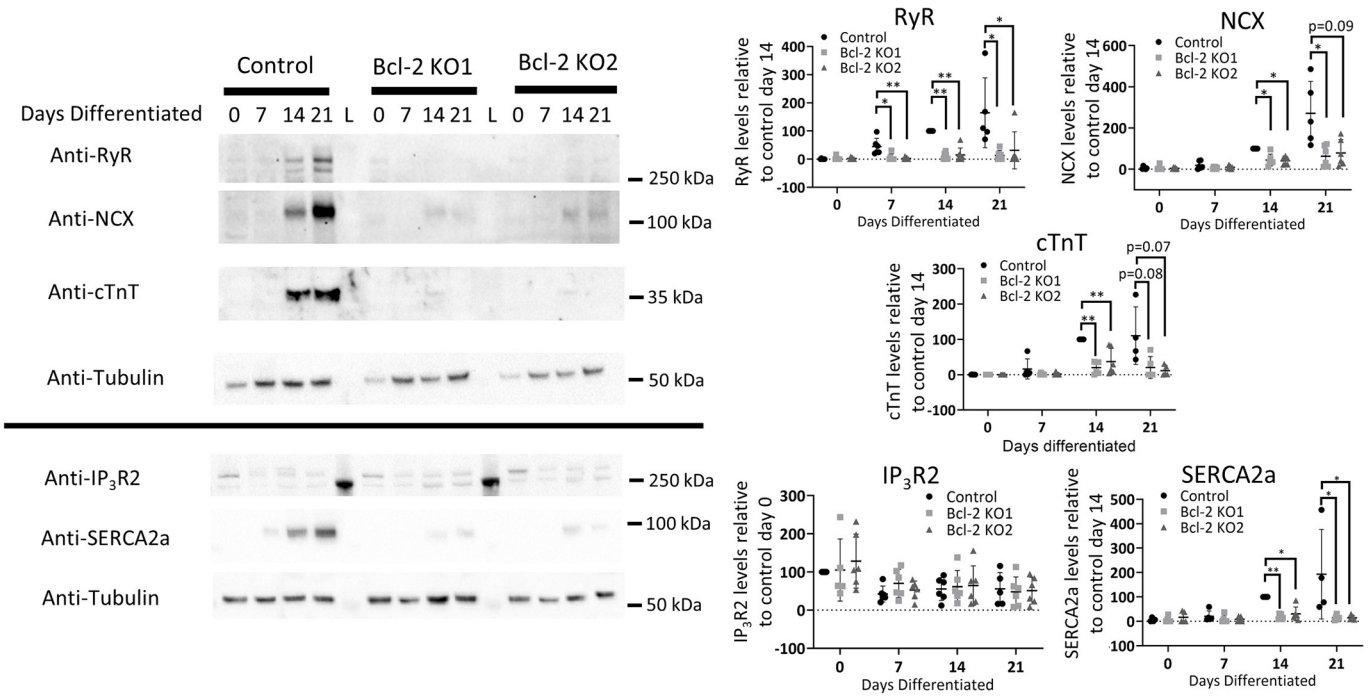

Fig. 5. KO of Bcl-2 impairs the expression of the cardiac Ca^{2+} toolkit. Left, immunoblot analysis of the indicated proteins in lysates prepared from cardiomyocytes derived from control or Bcl-2 KO clones differentiated for 0, 7, 14 or 21 days. The horizontal black line indicates which immunostainings were performed on the same immunoblot. L depicts the lane in which molecular mass markers were loaded. Right, quantification of the performed immunoblot experiments. All protein expression levels are normalized towards their corresponding loading control (tubulin) stained on the same membrane. All values were normalized to a control condition where expression levels were easily detected throughout the different experimental repetitions. For RyR, SERCA2a, cTnT and NCX this was control day 14; for IP_3R2 this was control day 0. Each data point represents an independent differentiation, which was performed at least four times ($n \geq 4$). The mean±s.d. are represented on the graphs. As the assumption for normal distribution were not met for all conditions, a non-parametric Kruskall–Wallis tests with Dunn's multiple comparison was performed *P<0.05; **P<0.01. P-values near to, but above, 0.05 are also shown.

Bcl-2 did not induce apoptosis or alter autophagic flux induction, but instead, resulted in delayed differentiation of cardiomyocytes from hiPSCs. Our data point towards a role for Bcl-2 in regulating early c-Myc stability, a transcription factor known to be required for cardiac differentiation and growth (Jackson et al., 1990).

It is known that Bcl-2 plays important roles during differentiation of neurons and cardiomyocytes, although the involved pathways remain to be fully elucidated (Liang et al., 2003; Limana et al., 2002; Kobayashi et al., 2006; Wei et al., 2005). In this study, we aimed to address this further and build on known functions of Bcl-2 in cardiomyocyte differentiation. To this end, a CRISPR/Cas9-mediated KO of Bcl-2 was generated in hiPSCs (Fig. 1). The CRSIPR/Cas9 assay was intended to introduce specific point mutations via homologous recombination in the *BCL2* gene, resulting in the introduction of a premature stop codon to prevent protein translation. Insertion of the selection cassette, which contained the mutations in the homology arm regions, was successful at the intended locus. However, after removal of the selection cassette none of the tested clones showed the introduction of the intended mutations. Rather, the majority of the clones showed a 4 base pair deletion at the sgRNA cut site, resulting in a frame shift and introduction of three premature stop codons, which effectively resulted in knocking out Bcl-2. The lack of protein was confirmed by immunoblotting, which showed a complete KO of Bcl-2 compared to the control line, indicating that these clones were suitable for use in this study.

After validating the KO of Bcl-2, the effects of lack of Bcl-2 on cardiomyocyte differentiation were addressed. In our differentiation of hiPSCs into cardiomyocytes, no change in expression of pluripotency or mesoderm markers was detected between conditions, suggesting that Bcl-2 KO was successful but also that the CRISPR/Cas9 editing did not have an impact on the early stages of the differentiation. However, a delay in the expression profile of four out of five tested early and late markers of cardiomyocyte differentiation was observed in Bcl-2 KO compared to controls (Fig. 2). This suggests that KO of Bcl-2 delays the differentiation of cardiomyocytes from hiPSCs at later stages in the differentiation and not by halting mesoderm induction. This conclusion was further supported by data from experiments in which we recorded spontaneous intracellular Ca^{2+} release. The occurrence, frequency and properties of these events are used as an index of cardiomyocyte differentiation and maturation (Fig. 4). From these experiments, it was clear that control cardiomyocytes showed increased spontaneous Ca^{2+} release over larger areas compared to that in the Bcl-2 KO conditions. However, when focused exclusively on the major regions of activity, no significant functional differences in the properties of the Ca^{2+} transients between control and Bcl-2 KO conditions could be detected. These results suggest that KO of Bcl-2 does not impair cardiomyocyte differentiation but rather influences the number of cells that successfully differentiate. This also fits well with the observation that Bcl-2 KO delays differentiation, which in turn limits the number of functional cardiomyocytes during the early stages of differentiation. A consideration here is that we are likely underestimating the effects of Bcl-2 KO on Ca^{2+} signalling as in these experiments because the decision to select an area for measurement was based on the presence of visual spontaneous activity. This spontaneous activity was much more pronounced in the control cardiomyocytes compared to in the Bcl-2 KO

Journal of Cell Science (2023) 136, jcs260216. doi:10.1242/jcs.260216

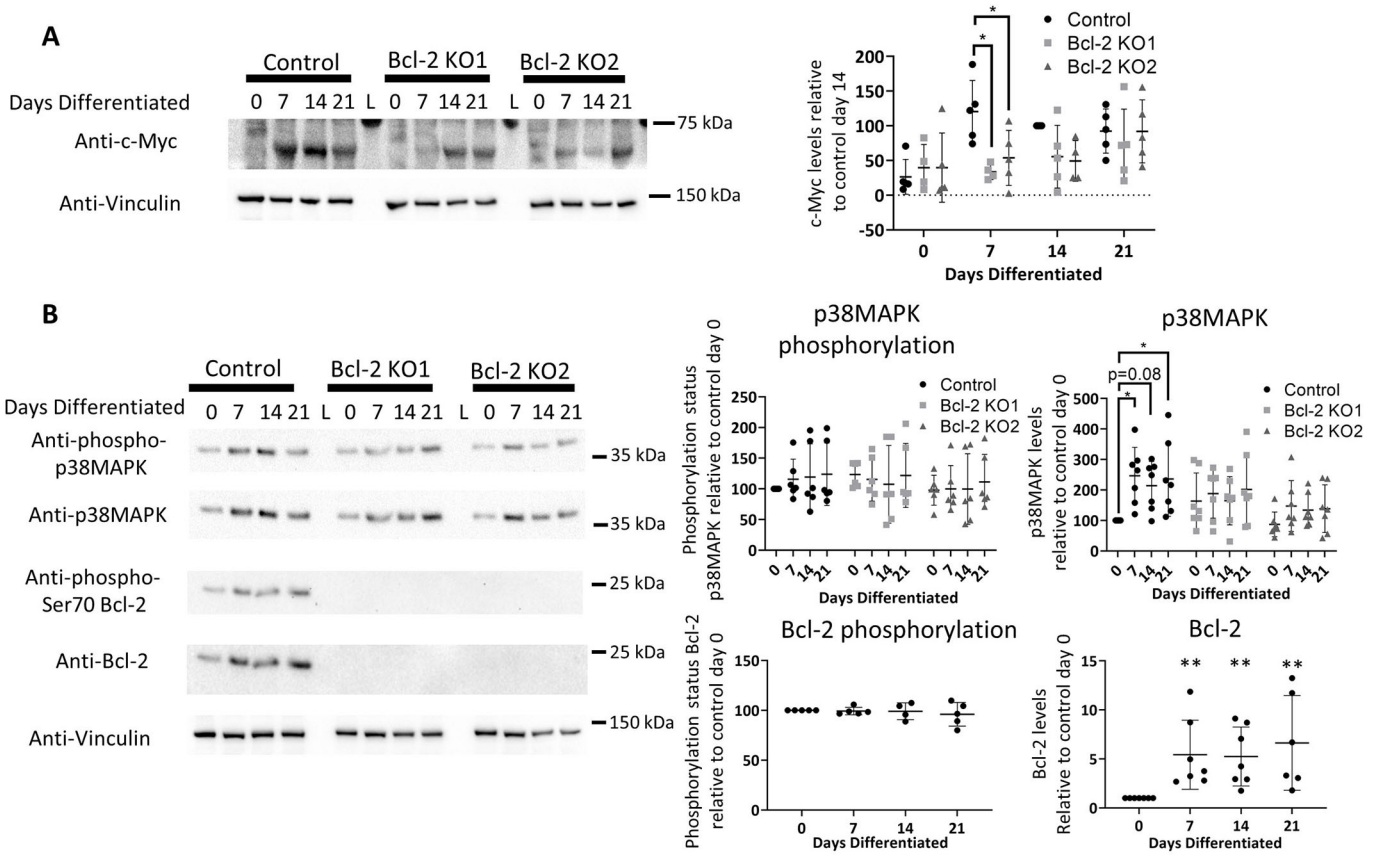

Fig. 6. Bcl-2 KO impairs upregulation of c-Myc. (A,B) Left, immunoblot analysis of cardiomyocytes derived from control or Bcl-2 KO clones differentiated for 0, 7, 14 or 21 days, stained for the indicated proteins. L depicts the lane in which molecular mass markers were loaded. Right, quantification of the performed immunoblot experiments. For quantifying the phosphorylation status of p38MAPK or Bcl-2, the protein levels detected by the phospho-antibody were normalized to the total amount of p38MAPK or Bcl-2. For all other quantifications, protein levels were normalized to their respective loading control (vinculin) and shown relative to a control condition where the protein was easily detected. For Bcl-2 and p38MAPK, this was control day 0; for c-Myc, this was control day 14. All differentiations were performed at least four times independently ($n \geq 4$). The mean±s.d. are represented on the graphs. In the conditions normalized to, the assumptions for normal distribution were not met. Therefore, when comparing these conditions Kruskall–Wallis tests with Dunn's multiple comparison were performed. All other conditions were normally distributed and allowed the use of one-way ANOVA tests with Tukey post test for multiple comparison. *P<0.05, **P<0.01. P-values near to, but above, 0.05 are also shown.

cardiomyocytes. As such, in the Bcl-2 KO conditions, we are likely sampling the subpopulation of the cells that differentiated properly and did not show large defects when specifically analysed.

The latter is further confirmed by the lack of expression of critical members of the cardiac Ca^{2+} toolkit in Bcl-2 KO cardiomyocytes (Fig. 5). These immunoblots monitor the average of the entire differentiating population. Based on the largely absent RyR, cTnT, SERCA2a and NCX in the Bcl-2 KO conditions, it could be expected that no spontaneous activity would be detected in the Bcl-2 KO lines. Nevertheless, a subpopulation of these cells was still able to produce spontaneous Ca^{2+} reactivity and contractions (Fig. 4). Furthermore, Bcl-2 KO did not result in excessive induction of apoptosis or changes in autophagic flux (Fig. 3). Taken together, these results indicate that Bcl-2 KO delayed differentiation, thereby limiting the number of functional cardiomyocytes without affecting their viability. This observed delay in differentiation might be a more general function of Bcl-2, not only restricted to cardiomyocytes, as Bcl-2 KO mice have severe growth retardation, which might be attributed to a general delay in differentiation when Bcl-2 is not present (Veis et al., 1993).

During cardiomyocyte differentiation, both p38MAPK and c-Myc activity play important roles in differentiation and growth. The p38MAPK family has been shown to act as a switch deciding between proliferation and differentiation of cardiomyocytes (Engel et al., 2005; Aouadi et al., 2006; Romero-Becerra et al., 2020). c-Myc expression in cardiomyocytes, on the other hand, is involved in cardiac growth (Jackson et al., 1990). Bcl-2 interacts with nuclear c-Myc, thereby regulating its transcriptional activity and stability (Jin et al., 2006). Bcl-2 translocation to the nucleus is dependent on its phosphorylation status (Zhou et al., 2017). p38MAPK phosphorylates Bcl-2 facilitating its translocation towards the nucleus (De Chiara et al., 2006). Other MAPK also phosphorylate Bcl-2. ERK1/2 for instance phosphorylates Bcl-2 at Ser70, thereby impacting its anti-apoptotic functions (Deng et al., 2000) and its functional cooperation with c-Myc (Jin et al., 2004), suggesting this is an important mechanism for several MAPK in the regulation of Bcl-2. Our results show that p38MAPK is active and able to phosphorylate its targets before and during differentiation of both control and Bcl-2 KO conditions (Fig. 6B). Under control conditions, Bcl-2 was phosphorylated and upregulated as has been previously described (Kobayashi et al., 2006). Together with Bcl-2, c-Myc levels were significantly higher at day 7 in control compared to KO conditions (Fig. 6A,B). Prolonged differentiation resulted in recovery of c-Myc levels towards control levels in both KO lines. Looking more closely at the localization of c-Myc at day 7 revealed that c-Myc levels in the nucleus were reduced in the Bcl-2

Journal of Cell Science (2023) 136, jcs260216. doi:10.1242/jcs.260216

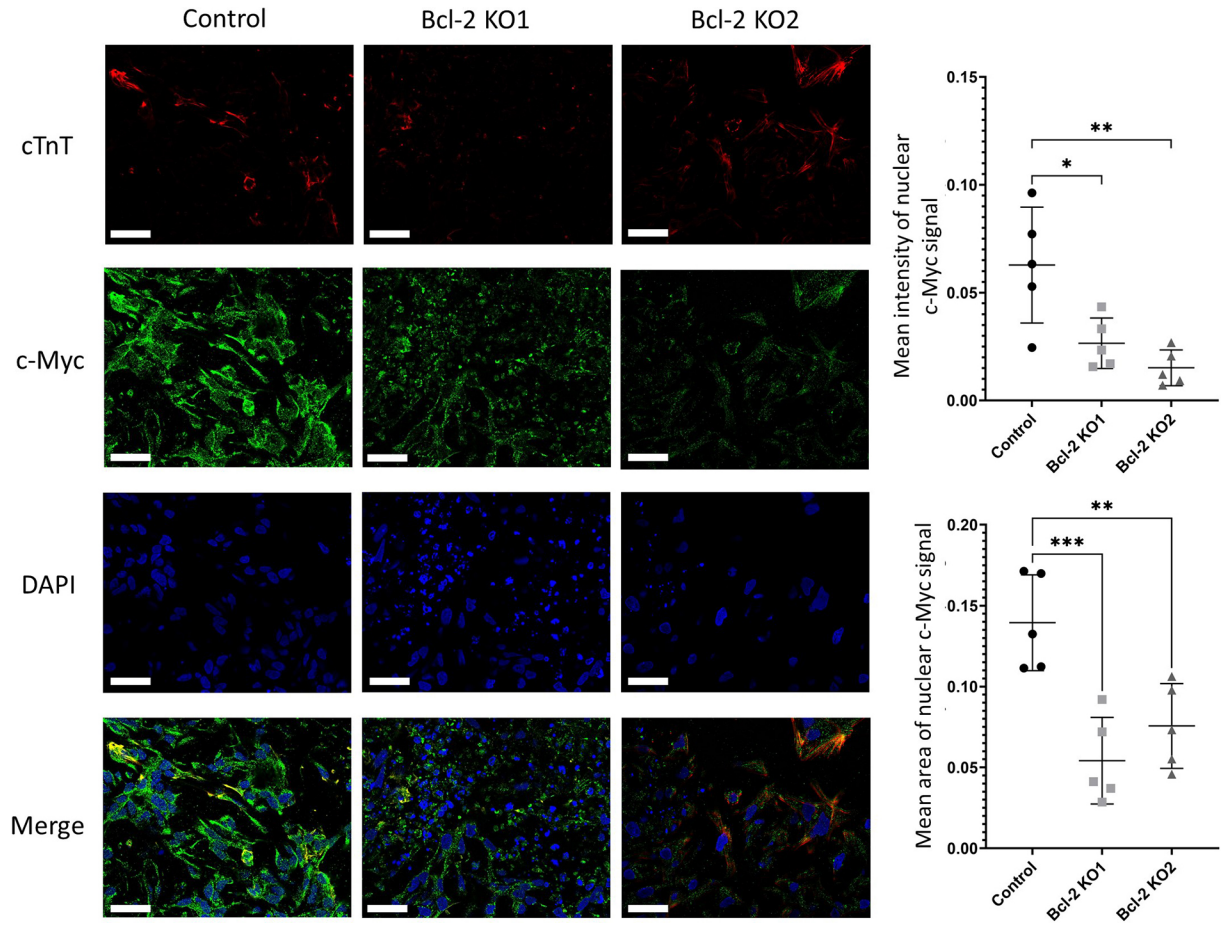

Fig. 7. KO of Bcl-2 reduces nuclear c-Myc localization. Left, confocal images of control and Bcl-2 KO cardiomyocytes differentiated for 7 days loaded with DAPI and immunofluorescently stained for cTnT and c-Myc. Scale bars: 20 µm. Right, quantification of the intensity (top) and area (bottom) occupied by nuclear c-Myc. Each data point indicates the mean±s.d. intensity or area of the c-Myc stain of all nuclei in one experimental day. The experiments were performed five times independently (n=5). All conditions were normally distributed allowing the use of one-way ANOVA test with Tukey post test for multiple comparison. *P<0.05, **P<0.01, ***P<0.001.

KO conditions compared to controls (Fig. 7). Given that c-Myc positively regulates the expression of many genes (Patel et al., 2004), it is logical to deduce that reducing c-Myc levels would result in a reduction of c-Myc-driven transcription and in turn reduced cardiac differentiation. Recently, it has been shown that the transcriptional output of c-Myc in the heart, following upregulation of c-Myc, is largely dependent on the presence of transcriptional cofactors that determine which genes will be activated (Bywater et al., 2020). In our hands, we demonstrated a reduction in the abundance of c-Myc upon Bcl-2 KO, suggesting that the lack of cofactors would not be an issue in this setting. However, in the context of cardiac differentiation of the Bcl-2 KO hiPSCs, these cardiac specific cofactors are expected to direct the limited amount of c-Myc towards genes necessary for differentiation, thereby allowing this process to occur at a slow or delayed rate compared to that in the control condition. The low amount of c-Myc still available in the Bcl-2 KO conditions might, at least in part, explain the delay, and not a complete halt, in differentiation observed upon Bcl-2 KO.

In summary, our results indicate that Bcl-2 is required for maintaining the temporal trajectory of early cardiomyocyte differentiation by regulating c-Myc expression and localization to the nucleus. Given the importance of c-Myc for cardiac differentiation, in combination with the lack of effect of Bcl-2 KO on expression of pluripotency markers and mesoderm induction, we propose that this Bcl-2-dependent decline in c-Myc dysregulated the expression of cardiac-specific genes. Specifically, loss of Bcl-2 resulted in delayed differentiation of cardiomyocytes from hiPSCs by lowering nuclear c-Myc signalling resulting in less efficient accumulation of functional cardiomyocytes.

MATERIALS AND METHODS

Reagents and antibodies

Unless otherwise specified, all chemicals were purchased from Merck (Hoeilaart, Belgium). Primary antibodies were anti-Vinculin (#V-9131), anti-c-Myc (#M4439, Merck), anti-Tubulin (#556321, BD Pharmingen, Erembodegem, Belgium) anti-Bcl-2 (#sc7382HRP), anti-phospho Ser70-Bcl-2 (#sc-293128, Santa Cruz, Heidelberg, Germany), anti-phospho-p70 S6 kinase (#9234S), anti-p70 S6 kinase (#9202), anti-phospho-p38MAPK (#9215S), anti-p38MAPK (#9212), anti-Bcl-X_L (#2764), anti-PARP (#9532S, Cell Signalling, Leiden, The Netherlands), anti-LC3 (#0231-100/LC3-5F10, Nanotools, Teningn, Germany), Anti-RyR (C3:33) (#MA3-916), anti-NCX (#MA3-926, Thermo Fisher Scientific, Waltham, MA, USA), anti-cTnT (#ab209813, Abcam, Cambridge, United Kingdom), anti-IP_3R2 (#R2872-2, Abiocode, Agoura Hills, CA, USA) and anti-SERCA2a (produced and kindly gifted by Prof. Frank Wuytack, KU Leuven, Belgium). More information concerning antibody dilution and validation/references can be found in Table S1. All primers and gene blocks used in this

study were purchased from integrated DNA technologies (IDT; Leuven, Belgium). Primers are listed in Tables S2 and S3.

hiPSC culturing

All experiments were performed using the commercially available Gibco™ Episomal hiPSC line (A18945; Thermo Fisher Scientific), which was regularly tested for presences of mycoplasma. hiPSCs were cultured feeder-free on Geltrex LDEV-Free hESC-Qualified Reduced Growth Factor Basement Membrane Matrix (Thermo Fisher Scientific; #A1413201) and maintained in Essential 8 Flex Basal Medium supplemented with Essential 8 Flex Supplement and 0.1% penicillin-streptomycin (all from Thermo Fisher Scientific), at 37°C under normoxic conditions (21% O_2 and 5% CO_2). Medium was changed daily. Colonies were routinely passaged non-enzymatically with 0.5 mM EDTA in phosphate-buffered saline (PBS) (Thermo Fisher Scientific).

Cardiomyocyte differentiation of hiPSCs

For inducing cardiac differentiation, the iPSC cardiomyocyte differentiation kit (Thermo Fisher Scientific; #A2921201) was used according to the manufacturers protocol. Briefly, prior to differentiation, hiPSCs were seeded on a thin Matrigel™ Growth Factor Reduced (GFR) Basement Membrane Matrix layer (Merck; #CLS356252) and cultured for 3 days in Essential 8 medium at 37°C under hypoxic conditions (5% O_2 and 5% CO_2) until the cells reached ∼60% confluency. Cardiomyocyte differentiation was started after the addition of a mesoderm-inducing medium (medium A; day 0) for 48 h. After 24 h, cells were transferred from hypoxia to normoxia. At day 2 of differentiation, cells were incubated for another 48 h with a cardiomyocyte progenitor medium (medium B). From day 4 onwards, medium was changed every other day with cardiomyocyte maintenance medium. All experiments performed were approved by the Research Ethical Committee of UZ/KU Leuven (protocol number S62524).

Cloning of gRNA and selection plasmid

The *BCL2*-targeting sgRNA (forward: 5′-GAGAACAGGGTACGA-TAACC-3′ and reverse: 5′-GGTTATCGTACCCtGTTCTC-3′) was cloned in the pU6-(BbsI)CBh-Cas9-T2A-mCherry, a (Addgene plasmid #64324; deposited by Ralf Kuehn; Chu et al., 2015), using the BbsI restriction enzyme. In order to introduce a hygromycin selection cassette into the genomic *BCL2* sequence, two genomic DNA sequences, in close proximity and on either side of a TTAA sequence within 500 bp of the *BCL-2* sgRNA, were identified. These sequences [one 430 bp (HAL sequence; see Table S4) and a 450 bp long (HAR sequence)] were introduced using the NEBuilder® HiFi DNA Assembly Master Mix (New England BioLabs) in combination with the sequences produced as gene blocks (IDT) and the PiggyBAC-Hygro-TK vector flanking the Hygromycin resistance gene restricted with BamHI enzyme. In the HAR sequence, containing the start of the *BCL2* open reading frame, base pair substitution was incorporated in order to generate premature stop codons in the *BCL2* gene resulting in the knock-out.

CRISPR/Cas9-mediated knockout of *BCL2*

Transfection of hiPSC was performed by nucleofection using the commercially available Cell Line Nucleofector Kit (Lonza) according to their protocol. For the nucleofection, 2 µg of the sgRNA containing plasmid and 8 µg of the selection plasmid were utilized. After nucleofection, the hiPSC were plated onto Geltrex coated culture plates. On the third day after nucleofection, 50 ng/ml hygromycin was added to the medium to start the selection procedure. After 7 days of selection, single colonies were picked. The medium was refreshed each day with Essential 8 medium containing 50 ng/ml hygromycin until the colonies were sufficiently grown, after which cells were passaged. At this point, a fraction of the hiPSC was taken for genomic DNA isolation to screen for the insertion of the hygromycin selection cassette at the correct locus in the *BCL2* gene (see Table S2). Finally, in clones selected based on correct insertion of the hygromycin gene in the *BCL2* locus, the selection cassette was again removed. To this end, hiPSCs were detached and nucleofected with 5 µg of the PiggyBac transposase plasmid (kind gift of Prof. Catherine Verfaillie, KU Leuven, Belgium). The medium was changed daily using Essential 8 medium until cells reached 90% confluency. At this point fialuridine (FIAU; Merck) selection was started for 24 h to kill cells in which the selection plasmid was retained. After this, the cells were allowed to recover and grow with daily medium changes followed by single-colony picking. Finally, a complete gene editing-free Bcl-2 KO hiPSC line was obtained due to PiggyBac excision and FIAU selection. Once the colonies were amplified, genomic DNA was collected in order to screen for the absence of the selection cassette, modification in the *BCL2* gene and potential off-target genomic insertions or modifications (see Table S2).

Genomic DNA isolation

Genomic DNA was isolated using a PureLink™ Genomic DNA Mini Kit (Invitrogen) according to the manufacturer's protocol. The primers utilized for the subsequent PCRs can be found in Table S2. Sequencing of the PCR samples was performed by LGC genomics.

Immunoblot analysis

Cell pellets collected at 0, 7, 14 and 21 days of differentiation (500 ***g*** for 5 min) were resuspended on ice in lysis buffer [20 mM Tris-HCl pH 7.5, 150 mM NaCl, 1.5 mM $MgCl_2$, 0.5 mM DTT, 1% Triton X-100 containing both protease (EDTA free protease inhibitors, Thermo Fisher Scientific) and phosphatase (PhosSTOP, Roche) inhibitors], followed by further homogenizing using an Eppendorf douncer in order to facilitate lysis. Lysis was performed for at least 30 min with head over end mixing at 4°C followed by centrifugation for 5 min at 4°C at >5000 ***g***. The supernatant was collected, and protein concentration determined using a standard Bradford assay. Immunoblot samples were prepared at 0.5 µg/µl and were resolved by SDS-PAGE on 4–12% Bis Tris gradient gels (Thermo Fisher Scientific) and transferred to 0.45 µm PVDF (Merck) as described in Vervliet et al. (2014). Following this, primary antibody staining was performed overnight at 4°C and secondary antibody staining with HRP-conjugated antibodies (Bioke) was performed at room temperature for at least 2 h. Immunoreactive bands were visualized using Pierce™ ECL Western Blotting Substrate (Thermo Fisher Scientific) and imaged using a ChemiDoc™ MP imaging system (Bio-Rad). When the phosphorylation status of a protein was studied, the phospho-specific antibody was applied first. Prior to staining the total protein fraction on the same membrane. When required, the membranes were stripped utilizing the ReBlot Plus antibody stripping solution (Merck) according to the manufacturer's instructions. The full-length immunoblots merged with their colorimetric image are shown in Fig. S5.

RT-qPCR

RNA isolation was performed using a GenElute™ mammalian total RNA miniprep kit (Sigma) according to the manufacturer's protocol. After this, a DNA-free™ kit (Invitrogen) was used according to the manufacturer's protocol to remove potential contaminating genomic DNA. RNA concentrations were determined using a Nanodrop. cDNA was prepared by reverse transcription from 1000 ng total mRNA using the High Capacity cDNA reverse transcription kit (Applied Biosystems). For qPCR, forward and reverse primers for the genes of interest (see Table S3) were mixed with FastStart Universal SYBR Green Master (Rox; Roche). 5 µl of this mixture was pipetted in duplicate per condition in a 384-well plate after which 5 µl of a 1:10 dilution of the prepared cDNAs were added. Reactions were performed using a ViiA7 Real-Time PCR System (Thermo Fisher Scientific). For analysis, ΔΔCt values were determined for each condition using *GAPDH* and *RPL13A* as reference genes.

Immunofluorescence staining

Control and Bcl-2 KO cardiomyocytes were stained for cTnT after 14 days of differentiation and for c-Myc and cTnT after 7 days of differentiation. Briefly, the cells were fixed with 4% paraformaldehyde (PFA) for 10 min followed by permeabilization with 0.2% Triton X-100 in PBS containing 1% bovine serum albumin (BSA) for 15 min. Blocking of non-specific protein binding sites was performed for 1 h in 10% goat serum. Next, the cells were incubated overnight at 4°C with c-Myc and/or cTnT antibody followed by the appropriate Alexa Fluor 555 and/or Alexa Fluor 488

conjugated secondary antibody (Thermo Fisher Scientific; 4 µg/ml) for 1 h at 37°C. Confocal images were captured using a 63×1.4 NA oil immersion objective on a Zeiss LSM510 confocal microscope when cells were stained for cTnT alone. When imaging the co-staining of cTnT and c-Myc, a DAPI stain was also included in order to visualize the nuclei. Herein, additional confocal images were taken using a 63×1.4NA oil objective on a Zeiss LSM880-Airyscan AxioObserver confocal microscope. All microscope settings were kept identical when acquiring these images. Quantification of cTnT signal at day 14 of differentiation was performed using FIJI software. First, the background was subtracted. Next, the threshold for cTnT staining was determined on the control condition, which was utilized for all other conditions. After applying the threshold, the average intensity of the cTnT signal was measured focussing only on the cTnT-positive parts of each image. Quantification of the nuclear c-Myc signal at day 7 of differentiation was performed as follows. The images were converted into tiff format with separated channels. Nuclei were identified using Stardist (Weigert et al., 2020). Pyknotic nuclei were discarded based on size and shape features for all the image sets. Cellprofiler was used to analyse the differences in the intensity and area of c-Myc signal inside the nuclei (Stirling et al., 2021). To calculate intensities, background was subtracted from the c-Myc channel based on the lower-quartile-intensity of each image from *MeasureImageIntensity* module, and mean intensities per nuclei were calculated with *MeasureObjectIntensity* module in cellprofiler. To calculate area, the c-Myc was first identified as Objects with adaptive-threshold settings and typical diameter of objects set to 1–5 px, then they were converted into greyscale images using *ConvertObjectsToImage* module. The Area was finally calculated using *MeasureObjectIntensity* module to find the mean area of c-Myc per nuclei.

Intracellular Ca^{2+} imaging

Intracellular Ca^{2+} measurements were performed in hiPSC-derived cardiomyocytes differentiated for 9 or 11 days. In these experiments, cells were loaded with 1 µM of the Ca^{2+} reporter Fluo-4 AM (solubilized in cardiomyocyte maintenance medium) for 45 min in a humidified incubator at 37°C and 5% CO_2. Next, the cells were washed twice with cardiomyocyte maintenance medium, after which the dye was de-esterified for 45 min under the same conditions as for loading. Immediately prior to starting the Ca^{2+} imaging experiments, the maintenance medium was replaced with a pre-warmed (37°C) modified Krebs–Ringer solution (135 mM NaCl, 6.2 mM KCl, 1.2 mM $MgCl_2$, 12 mM HEPES, pH 7.3, 11.5 mM glucose and 2 mM $CaCl_2$). Additions were performed as indicated in the figure. Tetracaine was solubilized in the above modified Krebs–Ringer solution at 1 mM final concentration. Imaging was performed using a Nikon eclipse Ti2 inverted fluorescence microscope (Nikon) equipped with excitation filter FF01-378/474/554/635 and dichroic mirror FF01-432/515/595/730 and emission filter 515/30, all from Semrock. Excitation was performed at 470 nm using a CoolLed pR-4000 (CoolLed). Acquisition of the emitted fluorescent signal was performed at 10 Hz using a pco.edge 4.2bi sCMOS camera (pCO). For image analysis, FIJI software (Rueden et al., 2017) was utilized. To visualize fluorescence changes, a pseudo-line scan was first generated by re-slicing of the image stack at the location of a straight line that was drawn from top to bottom over the largest area of active hiPSC-derived cardiomyocytes. Profiles of fluorescence intensity were plotted and measured as indicated in the figures. To normalize for baseline fluorescence, traces are shown as F/F_0 where the F_0 value was obtained during the quiescent period after tetracaine administration. To determine the area of cells showing spontaneous Ca^{2+} activity, maximum intensity *Z*-projections were performed of the first 300 images per stack. A threshold for response was determined for one control condition in each experiment and applied to all other stacks. After thresholding, particle analyses were performed to determine the regions of interest, from which the size of the areas were calculated.

Cell death measurements

Cell death measurements were performed on hiPSC-derived cardiomyocytes differentiated for 0, 7, 14 and 21 days. 15 min before imaging, the cells were treated with a cell permeable Hoechst 33342 stain (2 µg/ml) (Merck), NucView®488 Biotium (1 µM) (Fremont, CA, USA) and propidium iodide (1 µg/ml) (Merck) in a modified Krebs–Ringer solution (135 mM NaCl, 6.2 mM KCl, 1.2 mM $MgCl_2$, 12 mM HEPES pH 7.3, 11.5 mM glucose and 2 mM $CaCl_2$). For each experiment, a control differentiation was treated for 5 h with 1 µM staurosporine (Tocris, Abingdon, UK) as a positive control for cell death induction. Imaging was performed using the above-mentioned Nikon eclipse Ti2 inverted fluorescence microscope (Nikon). For each image, excitation was performed consecutively at 360, 470 and 550 nm for Hoechst 33342, NucView®488 and propidium iodide, respectively. Microscope settings were kept the same on each experimental day. Quantification was performed using the FIJI software. Each experimental day, the staurosporine-treated condition was utilized to determine the threshold for positive NucView®488 and propidium iodide signal. Next, this threshold was applied to all other images and the number of NuncView®488 and/or propridium iodide positive nuclei were determined relative to the total number of nuclei given by the Hoechst 33342 stain.

Statistical analysis

Statistical analysis was performed using GraphPad Prism software (Version 9.1.1). All datasets were tested for normal distribution using Shapiro–Wilk tests. For normally distributed data sets showing insignificant variability between the conditions, depending on the dataset, one- or two-way ANOVA tests with Tukey or Dunnett post tests were performed, respectively. Non-normally distributed data sets were analysed using non-parametric Kruskall–Wallis tests. Additional information on the performed statistical tests can be found in the figure legends. If not otherwise specified, $P< 0.05$ was considered significant (with $P<0.05$, $P<0.01$, $P<0.001$ and $P<0.0001$ are designated as *, **, *** and ****, respectively).

Acknowledgements

The use of the Zeiss LSM 880 – Airyscan microscope at the Cell and Tissue Imaging Cluster, was supported by Hercules AKUL/15/37_GOH1816N and Fonds Wetenschappelijk Onderzoek (FWO) G.0929.15 to Pieter Vanden Berghe, University of Leuven.

Competing interests

The authors declare no competing or financial interests

Author contributions

Conceptualization: T.V.; methodology: T.V., R.D.; investigation: T.V., R.D., A.P. and R.L.R.; writing: T.V., R.D., L.R., M.S., A.P.; funding acquisition: T.V., H.L.R. and M.S.; supervision T.V., H.L.R. and M.S.

Funding

This work was supported by the Research Foundation-Flanders (Fonds Wetenschappelijk Onderzoek, FWO) 'krediet aan navorsers' (grant number: 1508319N) awarded to T.V. and a FWO research grant (grant number G066821N) awarded to M.S. T.V. is a recipient of a senior post-doctoral grant of the FWO (grant number: 12ZG121N). R.D. was supported by KU Leuven Rondoufonds voor Duchenne Onderzoek (EQQ-FODUCH-O2010) and KU Leuven Postdoctoral Mandate Type 1 (PDMT1/21/037). A.P. is supported by KULeuven C1 grant C14/21/093 awarded to H.L.R.

Data availability

All relevant data can be found within the article and its supplementary information.

Peer review history

The peer review history is available online at https://journals.biologists.com/jcs/lookup/doi/10.1242/jcs.260216.reviewer-comments.pdf

References

Aouadi, M., Bost, F., Caron, L., Laurent, K., Le Marchand Brustel, Y. and Binetruy, B. (2006). p38 mitogen-activated protein kinase activity commits embryonic stem cells to either neurogenesis or cardiomyogenesis. *Stem Cells* **24**, 1399-1406. doi:10.1634/stemcells.2005-0398

Blagosklonny, M. V. (2001). Unwinding the loop of Bcl-2 phosphorylation. *Leukemia* **15**, 869-874. doi:10.1038/sj.leu.2402134

Brunelle, J. K. and Letai, A. (2009). Control of mitochondrial apoptosis by the Bcl-2 family. *J. Cell Sci.* **122**, 437-441. doi:10.1242/jcs.031682

Bywater, M. J., Burkhart, D. L., Straube, J., Sabo, A., Pendino, V., Hudson, J. E., Quaife-Ryan, G. A., Porrello, E. R., Rae, J., Parton, R. G. et al. (2020). Reactivation of Myc transcription in the mouse heart unlocks its proliferative capacity. *Nat. Commun.* **11**, 1827. doi:10.1038/s41467-020-15552-x

Chu, V. T., Weber, T., Wefers, B., Wurst, W., Sander, S., Rajewsky, K. and Kuhn, R. (2015). Increasing the efficiency of homology-directed repair for CRISPR-Cas9-induced precise gene editing in mammalian cells. *Nat. Biotechnol.* **33**, 543-548. doi:10.1038/nbt.3198

De Chiara, G., Marcocci, M. E., Torcia, M., Lucibello, M., Rosini, P., Bonini, P., Higashimoto, Y., Damonte, G., Armirotti, A., Amodei, S. et al. (2006). Bcl-2 Phosphorylation by p38 MAPK: identification of target sites and biologic consequences. *J. Biol. Chem.* **281**, 21353-21361. doi:10.1074/jbc.M511052200

Deng, X., Ruvolo, P., Carr, B. and May, W. S.Jr. (2000). Survival function of ERK1/2 as IL-3-activated, staurosporine-resistant Bcl2 kinases. *Proc. Natl. Acad. Sci. USA* **97**, 1578-1583. doi:10.1073/pnas.97.4.1578

Engel, F. B., Schebesta, M., Duong, M. T., Lu, G., Ren, S., Madwed, J. B., Jiang, H., Wang, Y. and Keating, M. T. (2005). p38 MAP kinase inhibition enables proliferation of adult mammalian cardiomyocytes. *Genes Dev.* **19**, 1175-1187. doi:10.1101/gad.1306705

Jackson, T., Allard, M. F., Sreenan, C. M., Doss, L. K., Bishop, S. P. and Swain, J. L. (1990). The c-myc proto-oncogene regulates cardiac development in transgenic mice. *Mol. Cell. Biol.* **10**, 3709-3716. doi:10.1128/mcb.10.7.3709-3716.1990

Jin, Z., Gao, F., Flagg, T. and Deng, X. (2004). Tobacco-specific nitrosamine 4-(methylnitrosamino)-1-(3-pyridyl)-1-butanone promotes functional cooperation of Bcl2 and c-Myc through phosphorylation in regulating cell survival and proliferation. *J. Biol. Chem.* **279**, 40209-40219. doi:10.1074/jbc.M404056200

Jin, Z., May, W. S., Gao, F., Flagg, T. and Deng, X. (2006). Bcl2 suppresses DNA repair by enhancing c-Myc transcriptional activity. *J. Biol. Chem.* **281**, 14446-14456. doi:10.1074/jbc.M511914200

Kobayashi, S., Lackey, T., Huang, Y., Bisping, E., Pu, W. T., Boxer, L. M. and Liang, Q. (2006). Transcription factor gata4 regulates cardiac BCL2 gene expression in vitro and in vivo. *FASEB J.* **20**, 800-802. doi:10.1096/fj.05-5426fje

Liang, Y., Mirnics, Z. K., Yan, C., Nylander, K. D. and Schor, N. F. (2003). Bcl-2 mediates induction of neural differentiation. *Oncogene* **22**, 5515-5518. doi:10.1038/sj.onc.1206844

Limana, F., Urbanek, K., Chimenti, S., Quaini, F., Leri, A., Kajstura, J., Nadal-Ginard, B., Izumo, S. and Anversa, P. (2002). bcl-2 overexpression promotes myocyte proliferation. *Proc. Natl. Acad. Sci. USA* **99**, 6257-6262. doi:10.1073/pnas.092672899

Maundrell, K., Antonsson, B., Magnenat, E., Camps, M., Muda, M., Chabert, C., Gillieron, C., Boschert, U., Vial-Knecht, E., Martinou, J. C. et al. (1997). Bcl-2 undergoes phosphorylation by c-Jun N-terminal kinase/stress-activated protein kinases in the presence of the constitutively active GTP-binding protein Rac1. *J. Biol. Chem.* **272**, 25238-25242. doi:10.1074/jbc.272.40.25238

Patel, J. H., Loboda, A. P., Showe, M. K., Showe, L. C. and McMahon, S. B. (2004). Analysis of genomic targets reveals complex functions of MYC. *Nat. Rev. Cancer* **4**, 562-568. doi:10.1038/nrc1393

Pattingre, S., Tassa, A., Qu, X., Garuti, R., Liang, X. H., Mizushima, N., Packer, M., Schneider, M. D. and Levine, B. (2005). Bcl-2 antiapoptotic proteins inhibit Beclin 1-dependent autophagy. *Cell* **122**, 927-939. doi:10.1016/j.cell.2005.07.002

Romero-Becerra, R., Santamans, A. M., Folgueira, C. and Sabio, G. (2020). p38 MAPK pathway in the heart: new insights in health and disease. *Int. J. Mol. Sci.* **21**, 7412. doi:10.3390/ijms21197412

Rong, Y. P., Aromolaran, A. S., Bultynck, G., Zhong, F., Li, X., McColl, K., Matsuyama, S., Herlitze, S., Roderick, H. L., Bootman, M. D. et al. (2008). Targeting Bcl-2-IP_3 receptor interaction to reverse Bcl-2's inhibition of apoptotic calcium signals. *Mol. Cell* **31**, 255-265. doi:10.1016/j.molcel.2008.06.014

Rueden, C. T., Schindelin, J., Hiner, M. C., DeZonia, B. E., Walter, A. E., Arena, E. T. and Eliceiri, K. W. (2017). ImageJ2: ImageJ for the next generation of scientific image data. *BMC Bioinformatics* **18**, 529. doi:10.1186/s12859-017-1934-z

Stirling, D. R., Swain-Bowden, M. J., Lucas, A. M., Carpenter, A. E., Cimini, B. A. and Goodman, A. (2021). CellProfiler 4: improvements in speed, utility and usability. *BMC Bioinformatics* **22**, 433. doi:10.1186/s12859-021-04344-9

Veis, D. J., Sorenson, C. M., Shutter, J. R. and Korsmeyer, S. J. (1993). Bcl-2-deficient mice demonstrate fulminant lymphoid apoptosis, polycystic kidneys, and hypopigmented hair. *Cell* **75**, 229-240. doi:10.1016/0092-8674(93)80065-M

Vervliet, T., Decrock, E., Molgo, J., Sorrentino, V., Missiaen, L., Leybaert, L., De Smedt, H., Kasri, N. N., Parys, J. B. and Bultynck, G. (2014). Bcl-2 binds to and inhibits ryanodine receptors. *J. Cell Sci.* **127**, 2782-2792. doi:10.1242/jcs.150011

Vervliet, T., Parys, J. B. and Bultynck, G. (2016). Bcl-2 proteins and calcium signaling: complexity beneath the surface. *Oncogene* **35**, 5079-5092. doi:10.1038/onc.2016.31

Wei, L., Cui, L., Snider, B. J., Rivkin, M., Yu, S. S., Lee, C. S., Adams, L. D., Gottlieb, D. I., Johnson, E. M., Jr., Yu, S. P. and et al. (2005). Transplantation of embryonic stem cells overexpressing Bcl-2 promotes functional recovery after transient cerebral ischemia. *Neurobiol. Dis.* **19**, 183-193. doi:10.1016/j.nbd.2004.12.016

Weigert, M., Schmidt, U., Haase, R., Sugawara, K. and Myers, G. (2020). Star-convex Polyhedra for 3D Object Detection and Segmentation in Microscopy. 2020 Ieee Winter Conference on Applications of Computer Vision (Wacv) 3655-3662.

Zhou, M., Zhang, Q., Zhao, J., Liao, M., Wen, S. and Yang, M. (2017). Phosphorylation of Bcl-2 plays an important role in glycochenodeoxycholate-induced survival and chemoresistance in HCC. *Oncol. Rep.* **38**, 1742-1750. doi:10.3892/or.2017.5830